# A LINEAR SENSOR ARRAY WITH SELF-BENDING SENSITIVITY

*Jens Ahrens*[*]

Quality and Usability Lab
University of Technology Berlin
Ernst-Reuter-Platz 7
10587 Berlin, Germany
jens.ahrens@tu-berlin.de

*Ralf Vogelgesang*

Nano-Optics Group
Carl von Ossietzky University of Oldenburg
Ammerländer Heerstraße 114-118
26129 Oldenburg, Germany
ralf.vogelgesang@uni-oldenburg.de

## ABSTRACT

Self-bending wave fields exhibit an envelope that seemingly bends in space under free-field conditions. They are created by wave fronts that fold along a caustic. In this paper, we invert the concept by exploiting the reciprocity principle of the Helmholtz equation in order to create a linear sensor array whose sensitivity seemingly bends in free space in the nearfield of the array. The sensor array therefore allows for listening around a distracting source, a jammer, or a physical object as sensitivity nulls can be placed at a defined distance. We illustrate the operating range and the robustness of the solution based on numerical simulations. For the presented scenario, an attenuation of more than 50 dB in a controllable region in space is achieved in a frequency range of more than two octaves.

***Index Terms*—** sensor array, self-bending acoustic beams, nearfield beamforming, null steering

## 1. INTRODUCTION

Self-bending wave fields were first predicted in the field of quantum mechanics [1] and made their way to acoustics via optics [2]. In optics, a phase profile is imposed onto a beam of light via a phase mask, e.g. a transparent material of appropriately varying thickness [3]. The phase profile that is imposed is taken from an optical wave front that forms a caustic. A caustic occurs if the family of rays that represent the wave front exhibit an envelope and are tangent to that envelope. This envelope is then referred to as caustic. The same concept was applied to acoustic fields by [4, 5] using an array of acoustic transducers that controlled the phase profile of the evolving sound field.

Here, we propose to invert this concept to create a sensor array with self-bending sensitivity by exploiting the reciprocity of the Helmholtz equation. This allows for creating confined spatial regions of very low sensitivity so that the sensor array can listen *around* distracting sources, jammers, or obstacles that are located at a given distance.

A related concept in array beamforming is termed *null steering* [6, 7]. Here, the complex weights of a sensor array are designed such that the sensitivity of the entire array vanishes in a given direction. Typically, null steering is performed in the far-field regime and the weights of the individual elements of the array are determined via numerical optimization. A jammer that appears in the same direction like the target signal cannot be attenuated using this approach. Nearfield beamforming exploits the distance dependence of the curvature of wave fields so that nulls can be placed at a defined distance whereby it is typically assumed that the signal sources radiate spherical waves [8, 9, 10].

We propose a new category of nearfield beamformers that use a more advanced wave propagation model, which allows for designing the distance-dependent nearfield sensitivity of the array in a more explicit fashion. We use the example of an array of pressure microphones to illustrate the approach. The results hold for any array of isotropic sensors.

## 2. SELF-BENDING WAVE FRONTS

Non-spreading Airy wave packets were predicted in [1]. They were theoretical constructions in the original formulation as they exhibit infinite energy (similar to plane waves). Finite-energy approximations were then observed with light in [2]. In [4, 5], the concept was translated to acoustics and a method for creating a sound field that seemingly bends along a convex trajectory in free space without any external force was presented. Obviously, the wave itself is not accelerated. Rather, the amplitude envelope of the sound field appears to be bent. The concept of [4, 5] is illustrated in Fig. 1: A caustic is pre-defined along which the wave front folds. In the high-frequency limit, the wave front does not traverse the caustic. It is important to note that the self-bending waves evolve only in the high-frequency limit. This high-frequency limit is fulfilled if the considered wavelength is much smaller than the curvature of the caustic. More generally, any significant changes to the wave amplitude have to evolve at length scales much larger than the wavelength. Note that the caustic needs to be convex in order that the wave perfectly avoids a given region in the high-frequency limit.

We choose the sample caustic from [4], which is given by the cubic Bézier curve

$$B(t) = (1-t)^3 B_0 + 3t(1-t)^2 B_1 + 3(1-t)t^2 B_2 + t^3 B_3 \,, \quad (1)$$

with

$$B_0 = [0, -0.2311]^T, \qquad B_1 = [0.1, 0.0189]^T$$
$$B_2 = [0.25, 0.1689]^T, \qquad B_3 = [0.98, -0.3311]^T \,,$$

to allow for a direct comparison of the results. We limit our observations to the $x$-$y$-plane so that we define the four points that define the Bézier curve as $B_i = [x_i, y_i, 0]^T$. The red line in Fig. 1 illustrates (1). Note that the control variable $t$ does not represent the

[*]Jens Ahrens is supported by the German Academic Exchange Service (DAAD) and by grant AH 269/2-1 of the German Research Foundation (DFG).

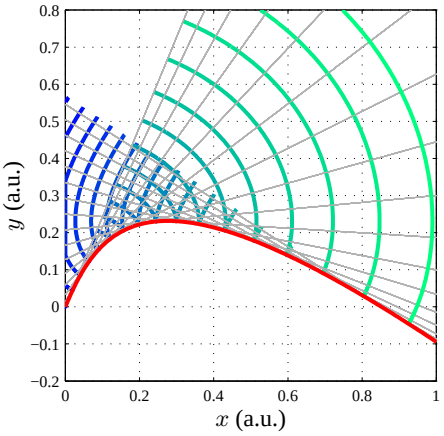


**Fig. 1**. Schematic of the principle of self-bending wave fronts; the red line indicates the prescribed caustic given by (1); the gray lines are sample tangents of the caustic; the blue/green lines are sample wave fronts; time may evolve from blue to green as well as from green to blue

traveled distance along $B(t)$, nor is it directly proportional to time when a wave moves along $B(t)$.

It is illustrated in [4] how the geometric wave fronts can be constructed from a preset beam trajectory via Legendre transformations. The wave fronts can then be traced back to a given reference plane on which their phases can be evaluated. For ease of illustration, we do not reproduce the analytic transformation but rather trace back the wave fronts numerically.

Once the phase profile of the desired wave field is known on the reference plane, i.e. on the plane on which the secondary sources are located, the appropriate secondary source driving signals can be determined via Rayleigh's first integral formula, which is given by [11]

$$P(\mathbf{x},\omega) = \iint_{-\infty}^{\infty} \underbrace{2\frac{\partial}{\partial \mathbf{n}} S(\mathbf{x},\omega)\big|_{\mathbf{x}=\mathbf{x}_0}}_{=D(\mathbf{x}_0,\omega)} G(\mathbf{x},\mathbf{x}_0,\omega) dA(\mathbf{x}_0) \,. \quad (2)$$

$P(\cdot)$ denotes the harmonic scalar wave field that evolves due to the monopole distribution along the reference plane. $G(\mathbf{x},\mathbf{x}_0,\omega) = \frac{1}{4\pi}\frac{e^{-\mathrm{i}\omega/c|\mathbf{x}-\mathbf{x}_0|}}{|\mathbf{x}-\mathbf{x}_0|}$ is the free-field Green's function, i.e. the spatio-temporal transfer function of the secondary monopole sources. $S(\cdot)$ is an arbitrary virtual scalar wave field that is source-free in the target half-space that is bounded by the reference plane. $dA(\cdot)$ is an infinitesimal surface element.

When the secondary monopoles are driven with two times the gradient $\partial/\partial\mathbf{n}$ of $S(\cdot)$ in direction normal to the boundary and evaluated at the boundary, then the synthesized wave field $P(\cdot)$ is identical to the virtual (prescribed) field $S(\cdot)$ inside the target half-space. It is proven in the Appendix that the driving signal $D(\cdot)$ is directly proportional to the phase of the harmonic field at the positions of the secondary sources.

It is therefore possible to create a self-bending wave by imposing the back traced phase profile of the self-bending wave onto a planar array of sufficiently densely spaced transducers. This approach is termed *phase engineering* [4, 5]. The amplitudes of the transducers are set equal in [4, 5].

Planar transducer arrays are inconvenient as the required number of elements is high. When wave field synthesis inside a given plane is targeted, then also linear arrays may be employed. The

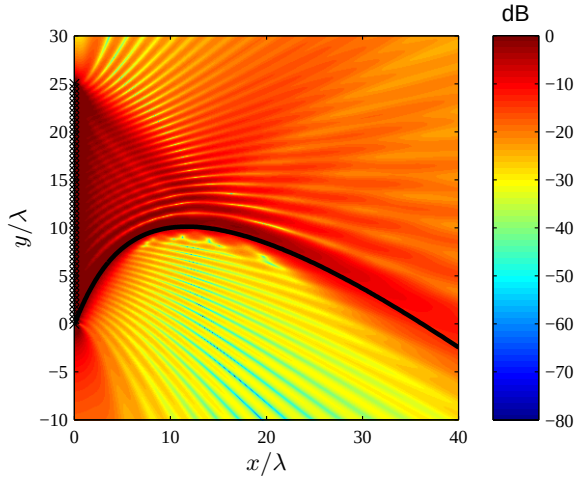


(a) Equal amplitude of 1 imposed on all array elements

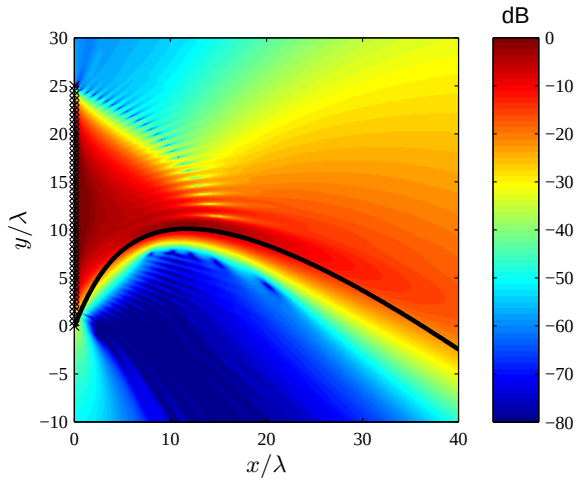


(b) Cosine-squared amplitude profile imposed on the array elements

**Fig. 2**. Sensitivity of a sample linear 51-element pressure-microphone array of length $L = 25\lambda$ located on the $y$-axis; the sensor spacing is $\Delta y = 0.5\lambda$; the black marks indicate the locations of the sensors; the black line represents the caustic; assuming a frequency $f = 2000$ Hz, this yields $\lambda \approx 0.17$ m, $L = 4.3$ m, $\Delta y = 0.086$ m

driving functions $D(\cdot)$ are identical to those for planar arrays apart from a global frequency dependent factor. This type of scenario is termed 2.5-dimensional and is well known in sound field synthesis [12]. The curvatures of the wave fronts that evolve are identical to the prescribed ones inside the target half-plane. The control over the amplitude decay of the synthesized field over distance to the array is limited. The synthesized wave field is obviously invariant with respect to rotation about the axis through the array's elements.

Refer to Fig. 2 for sample synthesized sound pressure fields based on the caustic that is defined by (1) and depicted in Fig. 1. The isotropic (monopole) transducer array extends along the $y$-axis. Fig. 3 depicts the phase profile that was imposed on the array elements. Fig. 2(a) shows the resulting sound field when all array elements exhibit equal amplitude. This corresponds to the approaches presented in [4, 5]. The attenuation in the quiet zone is in the order of 20 dB compared to locations along the caustic.

Phase engineering does not indicate the amplitude weights that

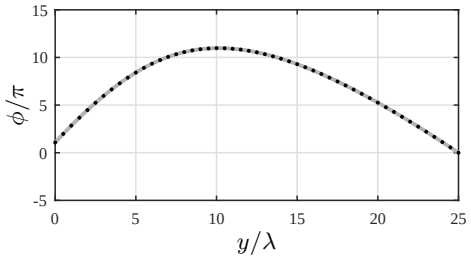


**Fig. 3**. Unwrapped phase profile $\phi(\cdot)$ of the arrays depicted in Fig. 2; the black marks indicate the values at the individual sensors

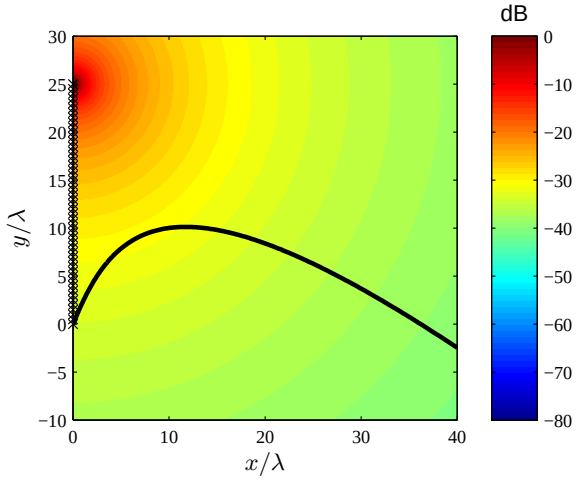


**Fig. 4**. Sensitivity of a single sensor with amplitude weight 1; all marks from Fig. 2 are included for orientation; the amplitude normalization is identical to Fig. 2

need to be applied to the transducers. Still, we may expect that the amplitudes of the transducers have significant impact on the sound field that evolves. Fig. 2(b) shows the resulting sound field when a cosine-squared shaped weighting is arbitrarily imposed on the array elements to show the effect. The difference to Fig. 2(a) is eminent. A pronounced quiet zone evolves south of the caustic indicated by the black line. The attenuation in the quiet zone is in the order of 60 dB compared to locations along the caustic.

The original experiments of self-bending optical fields are more similar to the scenario depicted in Fig. 2(b) rather than Fig. 2(a). In those experiments, the desired phase profile was imposed on Gaussian beams of light, which exhibit a bell-shape amplitude profile along their cross-section.

## 3. RECIPROCITY OF THE HELMHOLTZ EQUATION

Assuming stationary conditions and time-harmonic signals, the wave equation may be formulated conveniently in frequency domain. It is then referred to as *Helmholtz Equation* [11]. This formulation is particularly convenient as it exhibits a simple reciprocity relation: We may swap the source and the receiver positions in a given situation [13]. In the present context, we can replace the isotropic actuator array with an isotropic sensor array. The sensitivity of the sensor array to a monopole source in space is identical to the strength of the wave field caused by the actuator array at a given receiver location, assuming that the same phase and amplitude profiles are imposed on the actuators/sensors.

Formulated for the example of monopole sound sources and

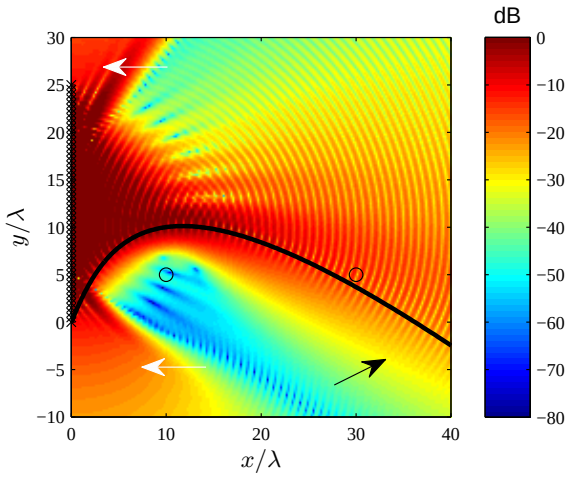


(a) The same scenario as in Fig. 2(b) but for a broadband signal covering two octaves; the black arrow indicates the impact of violating the high-frequency requirement; the white arrows indicate the impact of spatial aliasing; the color scale is identical to Fig. 2(b); the black circle mark the locations $\mathbf{x}_1$ and $\mathbf{x}_2$ that are evaluated in Fig. 6

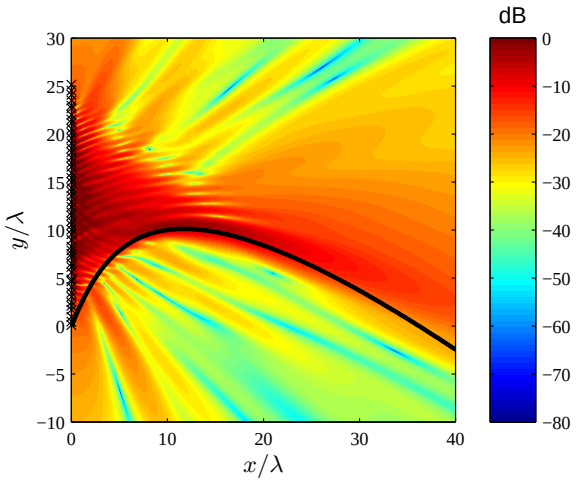


(b) The same (monochromatic) scenario as in Fig. 2(b) but with random displacement of the array elements along the $y$-axis according to a normal distribution with 0 mean and standard deviation of $0.2\Delta y$

**Fig. 5**. Sensitivity of a sample linear 51-element pressure-microphone array of length $L = 25\lambda$ located on the $y$-axis; the sensor spacing is $\Delta y = 0.5\lambda$; the black marks indicate the locations of the sensors; the black line represents the caustic

pressure microphones, this means that the amplitude of the sound pressure evoked by an array of monopole sources at a given location is identical to the sensitivity of a similar pressure microphone array to a monopole source at the considered location. Fig. 2 therefore depicts both scenarios. This equivalence was confirmed by the authors via numerical simulations.

## 4. RESULTS

The sensor array suppresses energy originating from sources that are located in the quiet zone. The most interesting observation is that the quiet zone does not extend along a line as it is the case in conventional farfield null steering [6, 7]. It is rather distance dependent

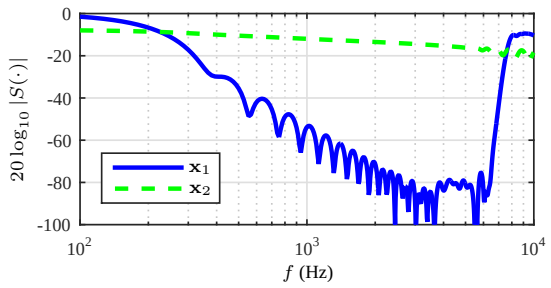


**Fig. 6**. Transfer functions from $\mathbf{x}_1 = (10, 5)$ and $\mathbf{x}_2 = (30, 5)$ to the output of the sensor array; the setup is identical to Fig. 5(a), i.e. the sensor spacing $\Delta y = \lambda/2$ at $f = 2000$ Hz; $\mathbf{x}_1$ and $\mathbf{x}_2$ are marked in Fig. 5(a)

so that energy from sources at a defined distance can be suppressed. In other words, we can listen around a jammer or around a physical obstacle. This capability is obvious when comparing the array sensitivity depicted in Fig. 2(b) to the sensitivity of any of the individual sensors that the array is composed of. Refer to Fig. 4, which shows the sensitivity of a single sensor with amplitude weight 1. The array's sensitivity can be several 10 dB higher than that of a single sensor in regions where a high sensitivity is desired and several 10 dB lower in regions where attenuation is desired. Note that the largest weight that was applied to the sensors in Fig. 2(b) is also 1.

The attenuation in the quiet zone that is achieved by the presented approach is well beyond that of conventional nearfield beamforming [8, 9, 10]. Note, however, that a comparison is difficult as the presented approach requires arrays that are significantly larger than those typically used in conventional nearfield beamforming.

### 4.1. Broadband Performance

Fig. 5 depicts the broadband performance of the array from Fig. 2(b). The absolute transducer positions are identical to Fig. 2(b), i.e. the spacing is a half wavelength at $f_{\text{ref}} = 2000$ Hz. A frequency range of two octaves between $0.4 f_{\text{ref}}$ and $1.6 f_{\text{ref}}$ was sampled at intervals of 20 Hz and the complex sensitivity was accumulated. The appropriate phase profile was determined for each frequency and the absolute sensor positions were fixed.

Reducing the frequency tends towards violating the high-frequency assumption underlying the approach so that more energy spills over into the quiet zone (black arrow in Fig. 5(a)).

Increasing the frequency beyond $f_{\text{ref}}$ violates the sampling criterion. Assuming that two sensors are required per wavelength, then the spatial aliasing frequency of the considered array is at $f = 2,000$ Hz. Actually, the sampling criterion for spatial sampling is somewhat more complicated as the resulting signal (the sensitivity) has more spatial dimensions than the sampled signal (the phase and amplitude profile of the array elements) [12]. Still, asking for two sampling points per wavelength is a convenient rule of thumb.

Interestingly, violating the sampling criterion does not immediately render void all efforts. It is rather such that side lobes arise for the directivity that point into directions that are at small angles to the array (white arrows in Fig. 5(a)). A similar observation was made in [4]. Note that the sampling criterion is violated by a factor of 1.6 in Fig. 5(a) yet maintaining acceptable performance.

Fig. 6 illustrates the broadband sensitivity over an even wider frequency range for 2 selected sound source locations. The distance-dependent sensitivity vanishes when the sampling criterion is violated by a factor of 3.5 or higher.

### 4.2. Robustness

The underlying filter-and-sum design of the beamformer provides good robustness [6, 7]. This is illustrated in Fig. 5(b), which depicts the same monochromatic scenario as is Fig. 2(b) but with a random displacement of the array elements along the $y$-axis according to a normal distribution with 0 mean and standard deviation of 20 % of the inter-element spacing $\Delta y$. Note that this constitutes a massive displacement. Yet, the array achieves an attenuation of several 10 dB in the quiet zone with respect to the most sensitive locations.

## 5. CONCLUSIONS

We proposed to invert the concept of self-bending wave fronts to create a nearfield sensor array with self-bending sensitivity. Such an array allows for listening around a distracting source or an obstacle. The approach for determining the phase profile that is imposed on the sensors was justified via Rayleigh's first integral formula. We illustrated that the sensors' amplitude profile can have substantial impact on the performance of the array. Robustness and broadband performance were also investigated. We showed that the attenuation in the quiet zone can be maintained even for sensor spacings that are slightly larger than half a wavelength.

## APPENDIX: DERIVATION OF THE SECONDARY SOURCE PHASE PROFILE

Consider the driving function $D(\mathbf{x}_0, \omega)$ for the secondary source at $\mathbf{x}_0$ to synthesize a sound pressure field $S(\mathbf{x}, \omega)$ as given by (2). The directional gradient $\frac{\partial}{\partial \mathbf{n}}$ is defined as [14]

$$\frac{\partial}{\partial \mathbf{n}} = \cos\alpha_{\text{n}} \sin\beta_{\text{n}} \frac{\partial}{\partial x} + \sin\alpha_{\text{n}} \sin\beta_{\text{n}} \frac{\partial}{\partial y} + \cos\beta_{\text{n}} \frac{\partial}{\partial z} \,, \qquad (3)$$

with $\alpha_{\text{n}}$ being the azimuth of the orientation of $\mathbf{n}$ and $\beta_{\text{n}}$ being the colatitude. For the present case of $\mathbf{n}$ pointing in positive $x$-direction, $\partial/\partial\mathbf{n}$ simplifies to $\partial/\partial x$.

Recall that we assume stationary conditions and time-harmonic signals in this paper. We may express $S(\mathbf{x}, \omega)$ as

$$S(\mathbf{x}, \omega) = A(\mathbf{x}, \omega) e^{\mathrm{i}\phi(\mathbf{x},\omega)} \qquad (4)$$

with purely real amplitude $A(\mathbf{x}, \omega) = |S(\mathbf{x}, \omega)|$ and purely real phase $\phi(\mathbf{x}, \omega) = \angle S(\mathbf{x}, \omega)$. Differentiation of (4) with respect to any of the Cartesian dimensions yields

$$\begin{aligned} \left(A(\mathbf{x}, \omega) e^{\mathrm{i}\phi(\mathbf{x},\omega)}\right)' &= A'(\mathbf{x}, \omega) e^{\mathrm{i}\phi(\mathbf{x},\omega)} + A(\mathbf{x}, \omega) \left(e^{\mathrm{i}\phi(\mathbf{x},\omega)}\right)' \\ &= \left[A'(\mathbf{x}, \omega) + A(\mathbf{x}, \omega)\mathrm{i}\phi'(\mathbf{x}, \omega)\right] e^{\mathrm{i}\phi(\mathbf{x},\omega)} \\ &\backsimeq A(\mathbf{x}, \omega)\phi'(\mathbf{x}, \omega) e^{\mathrm{i}\phi(\mathbf{x},\omega) + \mathrm{i}\frac{\pi}{2}} \,, \end{aligned} \qquad (5)$$

where in the last step we made use of the stipulated assumption that the high-frequency limit applies, i.e. $\left|\frac{\partial}{\partial \mathbf{n}} A(\mathbf{x}, \omega)\right| \ll \left|\frac{\omega}{c} \mathbf{n} A(\mathbf{x}, \omega)\right|$, which is known as the *eikonal approximation* [15].

Recall that (2) states that $D(\mathbf{x}_0, \omega) \propto \left(A(\mathbf{x}, \omega) e^{\mathrm{i}\phi(\mathbf{x},\omega)}\right)'\big|_{\mathbf{x}=\mathbf{x}_0}$. We can deduce from (5) that, in the high-frequency limit, the phase profile $\phi(\mathbf{x}_0, \omega)$ of the driving function $D(\mathbf{x}_0, \omega)$ is identical to the phase profile of the desired sound field on the secondary source contour and the term $A(\mathbf{x}, \omega)\phi'(\mathbf{x}, \omega)$ in (5) represents the (purely real) weight profile to be applied.

## 6. REFERENCES


[1] Michael V. Berry and Nandor L. Balazs, "Nonspreading wave packets," *A. J. Phys.*, vol. 47, no. 3, pp. 264–267, Mar. 1979.

[2] Georgios A. Siviloglou and Demetrios N. Christodoulides, "Accelerating finite energy Airy beams," *Optics Letters*, vol. 32, no. 8, Apr. 2007.

[3] Elad Greenfield, Mordechai Segev, Wiktor Walasik, and Oren Raz, "Accelerating light beams along arbitrary convex trajectories," *Phys. Rev. Lett.*, vol. 106, no. 213902, May 2011.

[4] Peng Zhang, Tongcang Li, Jie Zhu, Xuefeng Zhu, Sui Yang, Yuan Wang, Xiaobo Yin, and Xiang Zhang, "Generation of acoustic self-bending and bottle beams by phase engineering," *Nature Communications*, vol. 5, no. 4316, pp. 1–9, 2014.

[5] Sipei Zhao, Yuxiang Hu, Jing Lu, Xiaojun Qiu, Jianchun Cheng, and Ian Burnett, "Delivering sound energy along an arbitrary convex trajectory," *Scientific Reports*, vol. 4, no. 6628, pp. 1–6, 2014.

[6] Barry D. van Veen and Kevin M. Buckley, "Beamforming: A versatile approach to spatial filtering," *IEEE ASSP Magazine*, vol. 5, pp. 4–24, Apr. 1988.

[7] Harry L. van Trees, *Optimum Array Processing*, Wiley, New York, 2002.

[8] H. Lebret and S. Boyd, "Antenna array pattern synthesis via convex optimization," *IEEE Transactions on Signal Processing*, vol. 45, no. 3, pp. 526–532, Mar. 1997.

[9] J. R. Zheng, R. A. Goubran, and M. El-Tanany, "Robust near-field adaptive beamforming with distance discrimination," *IEEE Transactions on Speech and Audio Processing*, vol. 12, no. 5, pp. 478–488, Sept. 2004.

[10] Etan Fisher and Boaz Rafaely, "Near-field spherical microphone array processing with radial filtering," *IEEE TASL*, vol. 19, no. 2, pp. 256–265, Feb. 2011.

[11] Earl Williams, *Fourier Acoustics: Sound Radiation and Nearfield Acoustical Holography*, Academic Press, London, UK, 1999.

[12] Jens Ahrens, *Analytic Methods of Sound Field Synthesis*, Springer-Verlag, Berlin, Heidelberg, 2012.

[13] Philip M. Morse and Herman Feshbach, *Methods of Theoretical Physics*, Feshbach Publishing, Minneapolis, 1953 (reprinted 1981).

[14] George B. Arfken and Hans J. Weber, *Mathematical Methods for Physicists*, Elsevier Academic Press, Burlington, MA, sixth edition, 2005.

[15] Max Born and Emil Wolf, *Principles of Optics*, Pergamon Press, Oxford, UK, fourth edition, 1970.